LETTERS

# A 'granocentric' model for random packing of jammed emulsions

Maxime Clusel[1]*, Eric I. Corwin[1]*, Alexander O. N. Siemens[1] & Jasna Brujić[1]

**Packing problems are ubiquitous[1,2], ranging from oil extraction through porous rocks to grain storage in silos and the compaction of pharmaceutical powders into tablets. At a given density, particulate systems pack into a mechanically stable and amorphous jammed state[3,4]. Previous theoretical studies have explored a connection between this jammed state and the glass transition[4–8], the thermodynamics of jamming[9–12] and geometric modelling of random packings[13–15]. Nevertheless, a simple underlying mechanism for the random assembly of athermal particles, analogous to crystalline ordering, remains unknown. Here we use three-dimensional measurements of packings of polydisperse emulsion droplets to build a simple statistical model in which the complexity of the global packing is distilled into a local stochastic process. From the perspective of a single particle, the packing problem is reduced to the random formation of nearest neighbours, followed by a choice of contacts among them. The two key parameters in the model—the available space around a particle and the ratio of contacts to neighbours—are directly obtained from experiments. We demonstrate that this 'granocentric' view captures the properties of the polydisperse emulsion packing—ranging from the microscopic distributions of nearest neighbours and contacts, to local density fluctuations, to the global packing density. Application of our results to monodisperse and bidisperse systems produces quantitative agreement with previously measured trends in global density[16]. Our model therefore reveals a general principle of organization for random packing and may provide the foundations for a theory of jammed matter.**

Previous studies of the jammed state include characterizations of the network of forces[7,17–20], the packing microstructure[10–12,21,22], and effects of particle shape[23] and packing history[24]. In the following experiments, we visualize three-dimensional random packings of frictionless emulsion droplets using confocal microscopy to characterize the geometry and connectivity of the packing. Figure 1a presents an image of a fluorescently labelled oil-in-water emulsion, creamed under gravity to form a mechanically stable random pack (Methods). The confocal data are analysed using a deconvolution technique, which extracts the radius and position of each droplet with an accuracy of 1% of the average particle size (Methods). A typical probability distribution of radii $P(r)$, shown in Fig. 1b, exhibits a width of 23% of the mean radius. To characterize the local neighbourhood of each particle, we tessellate the packing using the navigation map[25], an extension of the Voronoi map to polydisperse systems. Each point in space is allocated to the particle whose surface is closest (Fig. 1c). Two particles are said to be neighbours if their corresponding cells share a common interface in the navigation map. Each cell in Fig. 1c is coloured according to the number of neighbours $n$ around the central particle, which ranges from 4 to 30. This wide range arises from the polydispersity of the sample and stands in contrast to the narrow range of nearest neighbours, typically from 12 to 17, of monodisperse systems[26].

A subset of the neighbours is in contact with the central particle and therefore capable of transmitting forces. The resulting network of forces gives rise to the mechanical stability of the packing. In the confocal images, points of contact between particles are self-consistently determined by the geometric overlap of spheres that reconstruct the particles and an intensity enhancement of the fluorescence of Nile Red dye[22] (Fig. 1a). We measure the mean number of contacts, also known as the coordination number, to be $\langle z \rangle = 6.3 \pm 0.3$, in good agreement with $\langle z_{iso} \rangle = 6$ required for isostatic mechanical equilibrium[27]. A slight discrepancy may be expected owing to the small deformation of the droplets.

While the global constraint of isostaticity is satisfied, the number of neighbours $n$ and contacts $z$ around each particle fluctuates significantly within the packing. Figure 1d shows that for each $n$, the number of contacts $z$ can take any value between 0 and $n$, which suggests that $z$ is randomly distributed. In addition, for particles with more neighbours the most likely number of contacts increases, indicated by the colour-coded probability map in Fig. 1d. Moreover, both $n$ and $z$ increase with the radius $r$ of the central particle, as shown in the scatter plot in Fig. 1e. This makes sense, as larger particles have more surface area available on which to fit neighbours.

To understand these observations, we consider the packing problem from the granocentric point of view of a single particle in the bulk, exemplified by the particle marked by a star in the confocal image in Fig. 1a. We propose a granocentric model for random packing, initially achieved by the formation of a set of neighbours, followed by the creation of contacts. This model allows for a definition of a local cell, giving access to the local packing fraction.

The starred particle in Fig. 1a is surrounded by 13 nearest neighbours. The space that each neighbour occupies depends on its size relative to the central particle. The space occupied by each neighbour around a central particle is characterized by the solid angle $\omega$ it subtends (Fig. 2a). Using this geometric description, we remove a trivial dependence of local packing on the central particle radius, which represents an important simplification. As shown in Fig. 2b, the packing of the neighbours precludes the addition of another neighbouring particle because there is a limited amount of available solid angle around the central particle, of radius $r_c$. This suggests an upper limit $\Omega_{max}(r_c)$ on the available solid angle.

We therefore model the formation of a set of $n$ nearest neighbours around a central particle of radius $r_c$ as a random selection of neighbours and a summation of their respective solid angles up to a threshold $\Omega_{max}(r_c)$. It follows that $n$ is the number of particles needed to reach, without exceeding, $\Omega_{max}(r_c)$. Following ref. 14, we ignore all neighbour–neighbour correlations by neglecting relative positions of neighbours on the surface of the central particle. The sizes of each

[1]Center for Soft Matter Research, Department of Physics, New York University, 4 Washington Place, New York, New York 10003, USA.
*These authors contributed equally to this work.

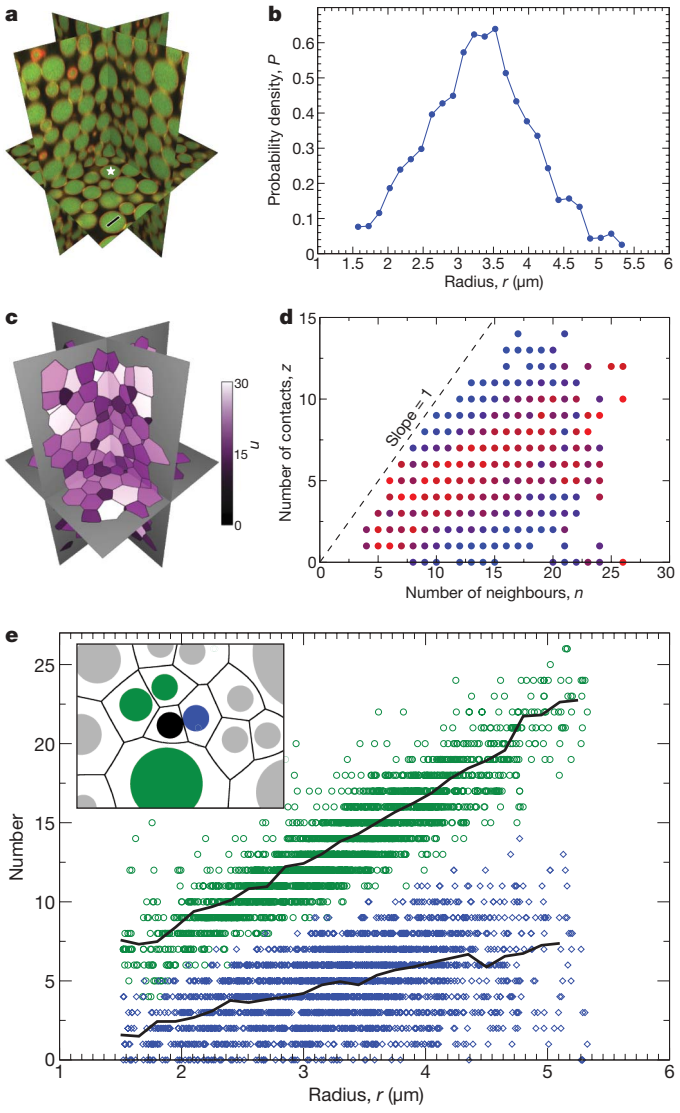


**Figure 1 | Microstructure of random polydisperse emulsions. a**, Projection of a three-dimensional confocal image of a creamed emulsion shows the emission fluorescence of droplets in green (505–570 nm) and the droplet contacts in yellow (575–640 nm). Scale bar, 5 μm. **b**, The distribution of droplet radii in this emulsion exhibits a mean of 3.3 μm and a standard deviation of 0.74 μm. **c**, Tessellation of the image in **a** according to the navigation map defines a local cell for each droplet, while the colour map indicates the number of nearest neighbours *n*. **d**, For a given *n*, the number of contacting neighbours *z* is shown as a scatter plot. The colour range from blue to red indicates an increasing probability of finding a particle with *z* contacts. **e**, The scatter plot shows the fluctuations in the number of contacts *z* (blue diamonds) and neighbours *n* (green circles) with droplet size, while their average values are shown to increase almost linearly (black lines). Inset, diagram illustrating the contacting neighbours of a droplet (blue) and those sharing an interface (green).

successive neighbour are therefore statistically independent and identically distributed. The formation of a set of neighbours thus corresponds to the first passage of a directed one-dimensional random walk, with steps given by the solid angles of the nearest neighbours (Fig. 2c).

In order to describe all the properties of a packing, knowledge of nearest neighbours must be supplemented by knowledge of the contact network responsible for mechanical stability. As noted in Fig. 1d, only a fraction of the *n* nearest neighbours are in contact with the central particle. The fluctuations in *z* shown in Fig. 1e suggest that contacts are randomly chosen among neighbours. We model the selection of contacts by Bernoulli trials with success rate $p(r_c)$, thereby neglecting all possible collective behaviour. Thus the distribution of the number of contacts *z* for a given number of neighbours *n*, $P(z|n)$, is a binomial distribution.

We have introduced two processes determining the connectivity of experimental packings. They are further characterized by fluctuations in the local packing fraction[11], which is relevant to global properties such as permeability and yield stress. The local packing fraction $\phi_{\mathrm{local}}$ is defined as the ratio of the particle volume $V_{\mathrm{particle}}$ to the cell volume $V_{\mathrm{cell}}$. As our granocentric model does not include information on neighbour positions, it is not possible to use the experimental definition of a cell in this framework. Instead, we use an effective definition for the local cell incorporating two salient physical features of the experimental cell: first, a particle with more neighbours will have a higher $\phi_{\mathrm{local}}$; second, for a given number of neighbours a particle with more contacts will have a higher $\phi_{\mathrm{local}}$. Therefore, we approximate the cell volume as the sum of the volume of the central particle plus the volumes contributed by a portion of space between the central particle and each of its neighbours (see Fig. 3c inset; a more complete description is given in Methods). The differing contribution to the cell volume by the neighbours and contacts is described by an effective surface-to-surface distance $\delta$, for non-contacting neighbours.

Thus, the statistical model reduces the packing problem complexity to two independent random processes at the single-particle level: first, the formation of a set of nearest neighbours is effected by assuming that the neighbours are chosen independently; second, the selection of contacts is assumed to be independent. The local definition of a cell provides further access to local packing fraction fluctuations. Whereas previous geometric models have predicted the average coordination number and density of discrete multicomponent systems[14,15], by mapping the packing problem onto the first passage of a random walk we are able to analytically study continuous distributions of radii and their influence on the full distributions of the number of nearest neighbours, coordination number and local density. Importantly, our model exploits the previously neglected observation that not all particles touch their neighbours.

Overall, the model introduces three parameters, $\Omega_{\max}(r_c)$, $p(r_c)$ and $\delta$, with different physical interpretations. The central parameter of our model, $\Omega_{\max}(r_c)$, is the available solid angle around a particle of radius $r_c$. It is an effective parameter whose value encompasses the details of the packing structure, such as polydispersity, steric effects, and long range correlations. For example, the available solid angle of a face-centred-cubic crystal is $3.2\pi$ owing to the space between neighbours, whereas the total solid angle around a sphere is $4\pi$. As described in Methods, the tools of random walks yield a functional relationship between the average number of neighbours around particles of radius $r_c$ and the threshold $\Omega_{\max}(r_c)$. Using the experimental average value of *n* for each radius $r_c$ presented in Fig. 1e, the model estimates $\Omega_{\max}(r_c)$. Remarkably, the experimentally determined values of $\Omega_{\max}(r_c)$ are independent of $r_c$ to within $\pm 0.15\pi$ around a value of $\sim 3.68\pi$. Thus, the ratio of the occupied surface area to the total surface area of the central particle does not depend on the size of the central particle in this polydisperse sample. The value of $3.68\pi$ is reasonable because it implies that there are unfilled spaces between the neighbours, observed in the example of Fig. 2b. The interpretation of $\Omega_{\max}$ as an upper limit is tested by directly measuring whether the total solid angle $\Omega_{\mathrm{tot}}$ around each particle lies below $\Omega_{\max}$. Figure 2d shows that 98% of the measured values are bounded by the estimated value of $\Omega_{\max}$, consistent with the proposed model assumptions.

To select contacts among neighbours, we introduced the success rate $p(r_c) = \langle z|r_c\rangle / \langle n|r_c\rangle$. There is no reason to suspect that this probability $p(r_c)$ should be independent of particle size. However, our measurements in Fig. 2e reveal that this average fraction of neighbours in contact is always $p(r_c) \approx 0.41$. This independence represents an important simplification and enhances the appeal of the model. We test the assumption that contacts are chosen independently by

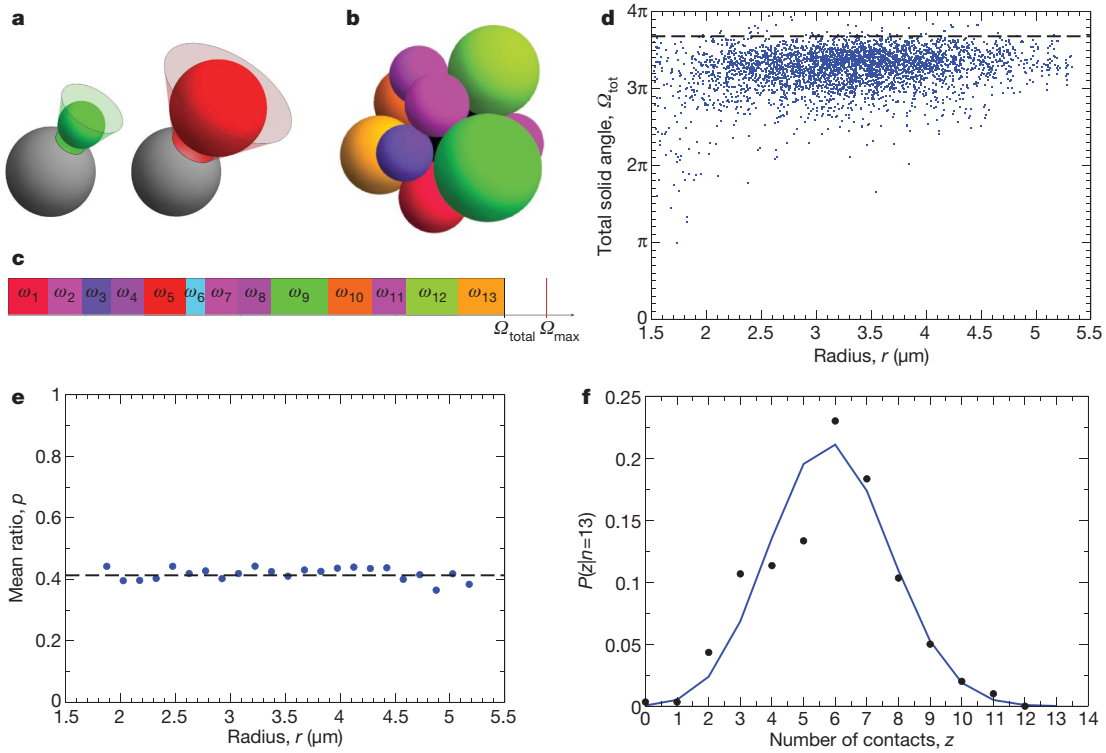


**Figure 2 | Granocentric view of random packing. a**, The space occupied by a neighbour around a central particle is measured by the solid angle it subtends, which is shown to depend on the neighbour size (green, smaller; red, larger). **b**, Nearest neighbours of the starred particle in Fig. 1a cover the surface of the central particle. **c**, Space-filling around the central particle in **b** is represented by a sum of the colour-coded solid angles $\omega$ occupied by each neighbour. **d**, A scatter plot of the total solid angle $\Omega_{tot}$ for each particle in the packing shows no dependence on the radius $r$ of the central particle. Consistent with the model prediction, almost all the points lie below the maximal solid angle $\Omega_{max} = 3.68\pi$, shown by the dashed line. **e**, Mean ratio of the number of contacts to neighbours, $p = \langle z/n \rangle$, is shown to be independent of $r$. **f**, For all particles with $n = 13$, the distribution of contacts $P(z|n)$ is consistent with a binomial distribution with a probability $p = 0.41$.

examining the experimental distribution of $z$ for a given $n$. As seen in Fig. 2f for $n = 13$, this distribution is captured by a binomial distribution with $p = 0.41$.

The final parameter in our model characterizes the local cell definition. The mean radius is a natural length scale in our system, which we use to quantify the effective distance $\delta$. We introduce a dimensionless parameter $\alpha$ such that $\delta = \alpha\langle r \rangle$, assumed to be the same for every non-contacting particle. We choose $\alpha = 0.30$ to match the experimentally measured mean local packing fraction. Thus, gaps between the neighbours are significantly smaller than the average particle size, consistent with the notion that one cannot fit further particles between a particle and its neighbour.

Using this framework, we calculate distributions of $n$, $z$ and $\phi_{local}$, and compare them with experimental results to test our model. Using the equations presented in Methods, we demonstrate in Fig. 3c that the predicted distributions are in excellent agreement with the experimental data. Furthermore, the full distributions as a function of the radius of the central particle are also shown to be in agreement (Supplementary Figs A–F). These results validate the model as a tool to predict the effects of polydispersity on random packings. As shown in Fig. 3b, both the experiments and the model show that 18% of particles are mechanically unstable, with fewer than four contacts. These particles, known as 'rattlers', arise naturally from the random packing processes of our model, in contrast to existing models that exclude rattlers and only focus on the network of contacts[24]. The agreement between model and experiment for local quantities $n$, $z$ and $\phi_{local}$ shows that the model quantitatively captures the local packing structure. The applicability of the model to packings with other size distributions is presented in Supplementary Information Section 4.0 and Supplementary Figs G–I. Numerical simulations show that the range of values for each parameter is narrow, but that the parameters are not universal for all polydispersities.

We can extend our local view of packing to predict the global density, a long-standing question in understanding random close packing[11,12,14,24,28,29]. The influence of the particle size distribution on global density has many industrial applications, such as predicting the density of dried paint or the density of porous rocks. The global packing fraction is defined as the ratio of the total volume of matter divided by the total volume of the sample. This is translated into our local model as:

$$\phi_{global} = \frac{\langle V_{particle} \rangle}{\langle V_{cell} \rangle} \quad (1)$$

It is important to note that the model value for the global packing fraction is relatively insensitive to the local fluctuations[14] and depends strongly only on $\alpha$. Using the model definition of the local cell volume, we predict the global density of our packings to within 0.5% of the experimentally measured 66.4%. It is not surprising that this polydisperse packing is denser than its monodisperse counterpart ($\phi_{global} \approx 64\%$)[24], as small particles can pack in the interstices of larger ones.

We further probe the predictive power of our model for systems with other size distributions by considering bidisperse packings. In such packings, polydispersity is a function of the size ratio of the two species and the volume ratio of all small particles to all particles. Using the local cell definition with the same parameters as for our experimental system, the model reproduces published experimental data[16] for different volume fractions of small particles and size ratios, even in the limit of the monodisperse case (Fig. 3d). This demonstrates that a local model based on geometric considerations alone provides an effective description of the packing as a whole.

The model accurately characterizes random, polydisperse packings in terms of numbers of nearest neighbours and contacts per particle,

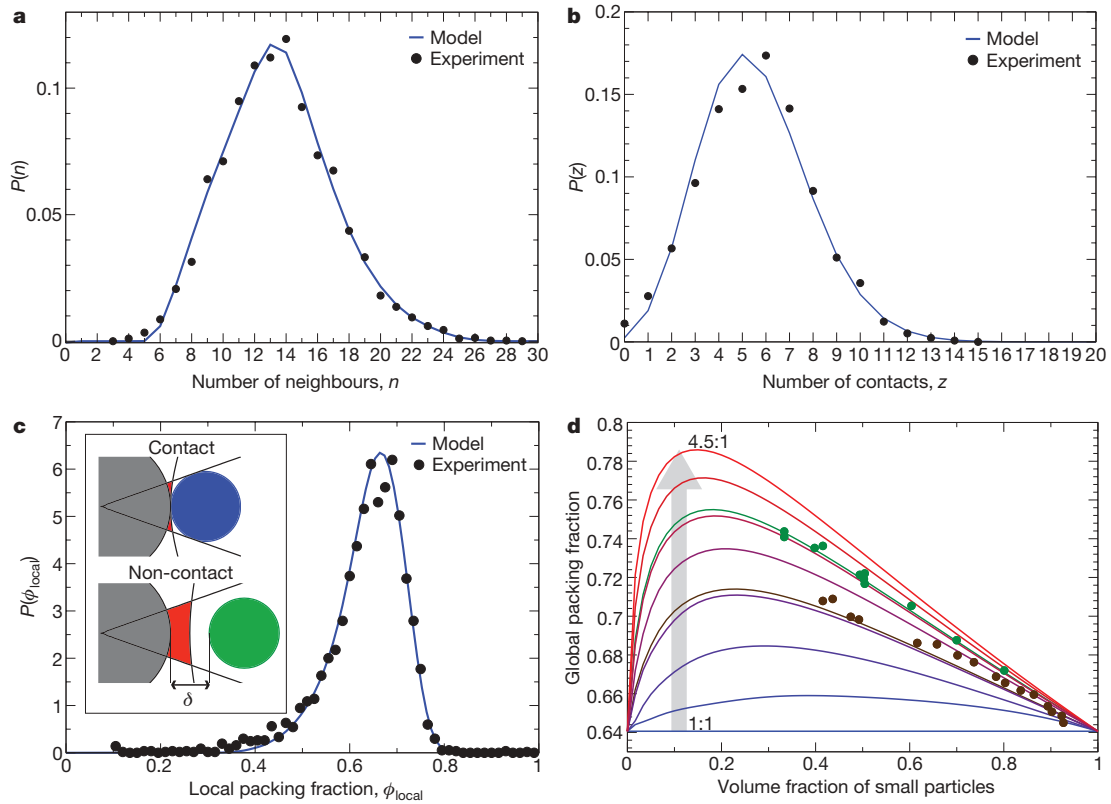


**Figure 3 | Comparison of model predictions with experiments.** **a**, **b**, The probability densities of the number of neighbours (**a**) and contacts (**b**) show excellent agreement between the experimental data and the statistical model. **c**, The probability density of the local packing fraction from the model successfully captures that obtained from the navigation map in Fig. 1c. Inset, volume contributions to the cell around each particle in the model. **d**, Model predictions for the global packing fraction of bidisperse systems are in good agreement with the experimental data reported[16] for size ratios of 2.58:1 (brown) and 3.41:1 (green). The lighter curves represent model predictions for size ratios ranging from 1:1 to 4.5:1 in increments of 0.5.

fluctuations in local density, and global density of the system. Our experiments reveal that the model parameters, $\Omega_{\max}$ and $p$, are independent of the central particle size, leading to a simple physical interpretation of the mechanism of random packing. From the perspective of each particle, a stable random packing is achieved when (1) the surrounding space is filled with a set of nearest neighbours and (2) some of those neighbours touch the central particle to achieve mechanical equilibrium. This model offers a simplified view of the packing problem, and opens an analytical path to explore the industrially important effects of polydispersity on local and global properties of packings.

It is surprising that such a simple model should describe the random packing of polydisperse spheres. For monodisperse packings, the only source of disorder is positional. Such a system is an archetypal example of a complex system, where correlations between particle positions determine the physical behaviour. In our system, the polydispersity serves as a second source of randomness added to the positional disorder. Our model is able to describe a polydisperse packing because the local source of randomness coming from the distribution of radii, $P(r)$, dominates the positional disorder.

The granocentric model can be used to count the number of equivalent local configurations in disordered packings, and thus may provide a definition for entropy. Thus, we may probe the contention that jammed packings can be described using a thermodynamic approach[9]. Other open questions that extensions to the model could answer include the effects of spatial dimensions and particle shape on packings. We have so far considered purely random packings, but it would be interesting to examine how correlations influence the microstructure, both in the model and in the experiments. This work represents an effective medium model for random close packing, while the determination of model parameters from first principles may provide a route to a complete theory.

## METHODS SUMMARY

**Mathematical methods.** The assumption that successive steps in the random walk are independent leads us to use the Laplace transform $\mathcal{L}$. If $X$ and $Y$ are two independent random variables of respective probability density $P_X$ and $P_Y$, then the probability density of the sum $P_{X+Y}$ satisfies $\mathcal{L}[P_{X+Y}] = \mathcal{L}[P_X]\ \mathcal{L}\ [P_Y]$. This basic observation, combined with standard probability tools, leads to the main results of this Letter.

Let $\omega = 2\pi\left(1 - \frac{1}{1+r/r_c}\sqrt{1+\frac{2r}{r_c}}\right)$ be the solid angle subtended by a particle of radius $r$ on a given central particle of radius $r_c$, where $r$ is drawn from the distribution $P(r)$. We compute $f_{r_c}(\omega)$, the probability density of solid angle around the central particle, by a change of variables from $P(r)$. The mean number of neighbours $\langle n|r_c\rangle$ around the central particle of radius $r_c$ is then given by

$$\langle n|r_c\rangle = \mathcal{L}^{-1}\left[\frac{1}{s}\frac{\mathcal{L}[f_{r_c}](s)}{1-\mathcal{L}[f_{r_c}](s)}\right](\Omega_{\max})$$

where $\mathcal{L}^{-1}$ is the inverse Laplace transform with respect to $s$, the conjugate variable of $\Omega_{\max}$. The probability density for a particle of radius $r_c$ to have $n$ neighbours given the maximal solid angle $\Omega_{\max}$, $P_{\text{neighbour}}(n;r_c, \Omega_{\max})$, is given by:

$$P_{\text{neighbour}}(n; r_c, \Omega_{\max}) = \mathcal{L}^{-1}\left[\frac{1-\mathcal{L}[f_{r_c}](s)}{s}\mathcal{L}[f_{r_c}](s)^n\right](\Omega_{\max})$$

Likewise, the distribution of coordination number $z$ can be computed as:

$$P_{\text{contact}}(z; r_c, \Omega_{\max}) = \mathcal{L}^{-1}\left[\frac{1-\hat{f}_{r_c}(s)}{s}\frac{\left(p\,\hat{f}_{r_c}(s)\right)^z}{\left(1-(1-p)\hat{f}_{r_c}(s)\right)^{z+1}}\right](\Omega_{\max})$$

**Definition of local cell.** The volume of a cell, $V_{\text{cell}}$, is defined as

$$V_{\text{cell}} = V_{\text{particle}} + \sum_{j=1}^{z} v_j + \sum_{j=1}^{n-z} v_j^*$$

where $v_j$ is the volume contribution of the $j$th contacting neighbour and $v_j^*$ is the volume contribution of the $j$th non-contacting neighbour. Let $\mathcal{C}$ be the cone subtended on the central particle by the neighbour particle in contact, and $\mathcal{S}$ be the surface of the central particle.

For contacting particles, let $\mathcal{H}$ be the surface of the hyperboloid defined by the navigation map of these two particles with surfaces in contact. The volume $v$ is defined as the volume of a region between the central particle and the neighbour that is the portion of $\mathcal{C}$ between $\mathcal{S}$ and $\mathcal{H}$.

For non-contacting particles, let $\mathcal{H}'$ be the surface of the hyperboloid defined by the navigation map of these two particles with surfaces separated by a distance $\delta$. The volume $v^*$ is then the portion of $\mathcal{C}$ between $\mathcal{S}$ and $\mathcal{H}'$.

**Full Methods** and any associated references are available in the online version of the paper at www.nature.com/nature.

**Received 2 April; accepted 12 May 2009.**


1. Jaeger, H. M., Nagel, S. R. & Behringer, R. P. Granular solids, liquids, and gases. *Rev. Mod. Phys.* **68,** 1259–1273 (1996).
2. de Gennes, P. G. Granular matter: a tentative view. *Rev. Mod. Phys.* **71,** S374–S382 (1999).
3. Cates, M. E., Wittmer, J. P., Bouchaud, J.-P. & Claudin, P. Jamming, force chains, and fragile matter. *Phys. Rev. Lett.* **81,** 1841–1844 (1998).
4. Liu, A. J. & Nagel, S. R. Nonlinear dynamics: jamming is not just cool anymore. *Nature* **396,** 21–22 (1998).
5. Barrat, A., Kurchan, J., Loreto, V. & Sellitto, M. Edwards' measures for powders and glasses. *Phys. Rev. Lett.* **85,** 5034–5037 (2000).
6. Coniglio, A., Fierro, A., Herrmann, H. J. & Nicodemi, M. (eds) *Unifying Concepts in Granular Media and Glasses: From the Statistical Mechanics of Granular Media to the Theory of Jamming* (Elsevier Science, 2004).
7. Corwin, E. I., Jaeger, H. M. & Nagel, S. R. Structural signature of jamming in granular media. *Nature* **435,** 1075–1078 (2005).
8. Parisi, G. & Zamponi, F. Mean field theory of the glass transition and jamming of hard spheres. Preprint at ⟨http://arXiv.org/abs/0802.2180⟩ (2008).
9. Edwards, S. & Oakeshott, R. Theory of powders. *Physica A* **157,** 1080–1090 (1989).
10. Lechenault, F., da Cruz, F., Dauchot, O. & Bertin, E. Free volume distributions and compactivity measurement in bidimensional granular packing. *J. Stat. Mech. Theory Exp.* P07009 (2006).
11. Aste, T. Volume fluctuations and geometrical constraints in granular packs. *Phys. Rev. Lett.* **96,** 018002 (2006).
12. Song, C., Wang, P. & Makse, H. A. A phase diagram for jammed matter. *Nature* **453,** 629–632 (2008).
13. Gotoh, K. & Finney, J. Statistical geometrical approach to random packing density of equal spheres. *Nature* **252,** 202–205 (1974).
14. Dodds, J. Simplest statistical geometric model of simplest version of multicomponent random packing problem. *Nature* **256,** 187–189 (1975).
15. Dodds, J. The porosity and contact points in multicomponent random sphere packings calculated by a simple statistical geometric model. *J. Colloid. Interface Sci.* **77,** 317–327 (1980).
16. Yerazunis, S., Cornell, S. & Wintner, B. Dense random packing of binary mixtures of spheres. *Nature* **207,** 835–837 (1965).
17. Liu, C. H. *et al.* Force fluctuations in bead packs. *Science* **269,** 513–515 (1995).
18. Brujić, J. *et al.* 3d bulk measurements of the force distribution in a compressed emulsion system. *Faraday Discuss.* **123,** 207–220 (2003).
19. Majmudar, T. & Behringer, R. Contact force measurements and stress-induced anisotropy in granular materials. *Nature* **435,** 1079–1082 (2005).
20. Zhou, J., Long, S., Wang, Q. & Dinsmore, A. Measurement of forces inside a three-dimensional pile of frictionless droplets. *Science* **312,** 1631–1633 (2006).
21. Bernal, J. Geometrical approach to the structure of liquids. *Nature* **183,** 141–147 (1959).
22. Brujić, J. *et al.* Measuring the coordination number and entropy of a 3d jammed emulsion packing by confocal microscopy. *Phys. Rev. Lett.* **98,** 248001 (2007).
23. Donev, A. *et al.* Improving the density of jammed disordered packing using ellipsoids. *Science* **303,** 990–993 (2004).
24. Torquato, S., Truskett, T. M. & Debenedetti, P. G. Is random close packing of spheres well defined? *Phys. Rev. Lett.* **84,** 2064–2067 (2000).
25. Richard, P., Oger, L. & Troadec, J.-P. A model of binary assemblies of spheres. *Eur. Phys. J. E* **6,** 295–303 (2001).
26. Finney, J. Random packings and structure of simple liquids. *Proc. R. Soc. Lond. A* **319,** 479–493 (1970).
27. Alexander, S. Amorphous solids: their structure, lattice dynamics and elasticity. *Phys. Rep.* **296,** 65–236 (1998).
28. Kamien, R. & Liu, A. Why is random close packing reproducible? *Phys. Rev. Lett.* **99,** 155501 (2007).
29. Aste, T., Saadaftar, M. & Senden, T. Local and global relations between the number of contacts and density in monodisperse sphere packs. *J. Stat. Mech. Theory Exp.* P07010 (2006).
30. Schmitt, V., Leal-Calderon, F. & Bibette, J. in *Topics in Current Chemistry* Vol. 227, *Colloid Chemistry II* (ed. Antonietti, M.) 195–215 (Springer, 2003).


**Supplementary Information** is linked to the online version of the paper at www.nature.com/nature.

**Acknowledgements** We thank G. Ben Arous, S. T. Bramwell, P. M. Chaikin, I. Z. Corwin, J.-B. Gouéré, P. C. W. Holdsworth, D. Levine, D. J. Pine and J. R. Royer for discussions and comments. J.B. holds a Career Award at the Scientific Interface from the Burroughs Wellcome Fund. This work was partially supported by NYU MRSEC Award DMR:0820341.

**Author Contributions** M.C. and E.I.C. contributed equally to this Letter and are listed in alphabetical order.

**Author Information** Reprints and permissions information is available at www.nature.com/reprints. Correspondence and requests for materials should be addressed to J.B. (jb2929@nyu.edu).

## METHODS

**Emulsion preparation and imaging.** The oil-in-water emulsion is prepared by mixing 3 vol.% Tergitol NP7 (nonyl phenolethoxy 7, Sigma) non-ionic surfactant with 3 wt% high viscosity Alginate HF120L (Promova) in 30 ml deionized water (Millipore), after the method of ref. 30. The disperse phase is composed of silicone oil (PDMS) droplets with varying viscosities, fluorescently labelled by Nile Red dye[18]. This mixture is injected into a narrow gap Couette mixer with a gap size of 100 μm and sheared between 18–22 r.p.m. A 16 mM solution of sodium dodecyl sulphate (SDS, Sigma) in a refractive index matched solution of water (50 wt%) and glycerol (50 wt%) infused with Nile Red dye is added to the creamed droplets.

The transparent emulsion is loaded into a sample cell, allowed to cream under gravity and analysed using a Leica SP2 confocal laser scanning microscope equipped with a high numerical aperture oil-immersion objective lens with a 100× magnification. The fluorescent dye is excited using a 488 nm argon laser and emission is detected using a photomultiplier behind a long-pass 500 nm filter with two channels.

**Image analysis.** The centre point and radius of each droplet was measured from the confocal images using a deconvolution technique that is well suited to measurements on jammed systems. Each droplet was considered as the convolution of a δ-function at its centre and a sphere of radius $r$. To make the measurements, we simply deconvolved the images to obtain the positions of all particles with a given radius $r$ using the following procedure.

A test 3D volume was created with a sphere of radius $r$ at its centre. Gaussian noise was added to this test particle with similar characteristics to the noise found in the confocal image. Both volumes were transformed into the frequency domain, where the Fourier transform of the confocal image was divided by the Fourier transform of the test volume. A tuned Wiener filter was applied to increase the signal relative to the noise. The resulting Fourier volume was then transformed back into the positional domain. In the resulting volume, numerical approximations to δ-functions marked the centre point of each droplet of radius $r$. This procedure was carried out for each radius $r$ until every droplet in the volume was located.